

# 1 Test Beam Studies Of Silicon Timing for Use in Calorimetry.

2 A. Apresyan<sup>a</sup>, G. Bolla<sup>b</sup>, A. Bornheim<sup>a</sup>, H. Kim<sup>c</sup>, S. Los<sup>\*,b</sup>, C. Pena<sup>a</sup>, E. Ramberg<sup>b</sup>,  
3 A. Ronzhin<sup>b</sup>, M. Spiropulu<sup>a</sup>, S. Xie<sup>a</sup>

4 <sup>a</sup>*California Institute of Technology, Pasadena, CA, USA*

5 <sup>b</sup>*Fermi National Accelerator Laboratory, Batavia, IL, USA*

6 <sup>c</sup>*University of Chicago, Chicago, IL, USA*

---

## 7 Abstract

8 The high luminosity upgrade of the Large Hadron Collider (HL-LHC) at CERN is ex-  
9 pected to provide instantaneous luminosities of  $5 \times 10^{34} \text{ cm}^{-2} \text{ s}^{-1}$ . The high luminosities  
10 expected at the HL-LHC will be accompanied by a factor of 5 to 10 more pileup compared  
11 with LHC conditions in 2015, further increasing the challenge for particle identification  
12 and event reconstruction. Precision timing allows to extend calorimetric measurements  
13 into such a high density environment by subtracting the energy deposits from pileup  
14 interactions. Calorimeters employing silicon as the active component have recently be-  
15 come a viable choice for the HL-LHC and future collider experiments which face very  
16 high radiation environments. In this article, we present studies of basic calorimetric and  
17 precision timing measurements using a prototype composed of tungsten absorber and sil-  
18 icon sensor as the active medium. We show that for the bulk of electromagnetic showers  
19 induced by electrons in the range of 20 GeV to 30 GeV, we can achieve time resolutions  
20 better than 25 ps per single pad sensor.

21 *Key words:*

22 Silicon, Timing, Calorimeter

---

## 23 1. Introduction

24 Future colliders, including the high luminosity upgrade of the Large Hadron Col-  
25 lider (HL-LHC) at CERN, will operate with an order of magnitude higher instantaneous  
26 luminosity compared to what has been achieved at the LHC so far. With the increased in-  
27 stantaneous luminosity the rate of simultaneous interactions per bunch crossing (pileup)  
28 is projected to reach an average of 140 to 200. The large amount of pileup increases the  
29 likelihood of confusion in the reconstruction of particles from the hard scatter interaction  
30 with those produced in different pileup interactions. The ability to discriminate between  
31 jets produced in the events of interests, especially those associated with the vector bo-  
32 son fusion processes, and jets produced by pileup interactions will be degraded. The

---

\*Corresponding author

Email address: los@fnal.gov (S. Los)

missing transverse energy resolution will deteriorate, and several other physics objects performance metrics will suffer.

One way to mitigate the pileup confusion effects, complementary to precision tracking methods, is to perform a time of arrival measurement associated with a particular layer of the calorimeter, allowing for a time assignment for charged particles and photons. Such a measurement with a precision of about 20-30 ps, when unambiguously associated to the corresponding energy measurement, will reduce the effective amount of pileup by a factor of 10, given that the spread in collision time of the pileup interactions at HL-LHC is foreseen to be approximately 200 ps. The association of the time measurement with the energy measurement is crucial, and leads to a prototype design that calls for time and energy measurements to be performed in the same detector element. Since both the energy and time measurement are performed in the same detector element<sup>1</sup>, once an energy deposit is identified as originating from a pileup interaction, it can be unambiguously removed from event reconstruction.

Several alternative options to combine high resolution energy and timing measurements for calorimetry have been reported in Refs. [1–5]. In this article, we describe the continuation of this program of study using a calorimeter prototype employing a 300  $\mu\text{m}$  thick silicon pad sensor of  $6 \times 6 \text{ mm}^2$  size as the active element. Silicon-based calorimeters have recently become a viable choice for future colliders due to the radiation hardness of silicon, and the ability to construct highly granular detectors. An important example is the forward calorimeter proposed for the CMS Phase 2 Upgrade [6, 7]. We study the timing properties of silicon-based calorimetry using a prototype composed of tungsten absorber and a silicon sensor produced by Hamamatsu [8].

The paper is organized as follows. General silicon timing properties and bench test results are described in Section 2. The test beam setup and experimental apparatus are presented in Section 3. The results of the test beam measurements are presented in Section 4. Sections 5 and 6 are devoted to discussion and conclusion, respectively.

## 2. General Properties of Silicon Timing and Bench Test Studies

For our measurements, we used a silicon sensor produced by Hamamatsu [8]. The thickness of the silicon was measured to be 325  $\mu\text{m}$ . The transverse size of the sensor is  $6 \times 6 \text{ mm}^2$ . The negative bias voltage was applied to the p-side of the silicon. The capacitance of the silicon diode is measured as a function of the bias voltage and shown in Figure 1. We observe that the silicon is fully depleted above about 120 V. Timing measurements are expected to improve with larger bias voltage as the carrier velocity increases.

The electric diagram of the silicon diode connections is presented in Figure 2. Attention was paid to provide good filtering for bias voltage, to reduce ground loop effects, and to minimize inductive loop for the signal readout. The timing characteristics of the signal pulses are dominated primarily by properties of the silicon sensor rather than the details of the circuit.

The silicon diode was placed inside a light-tight box of thickness 1.5 cm, which also provides electromagnetic shielding. The box is made of 0.2 mm steel. The bias voltage

---

<sup>1</sup>If there are no overlapping energy deposits in the same detector element from multiple particles.

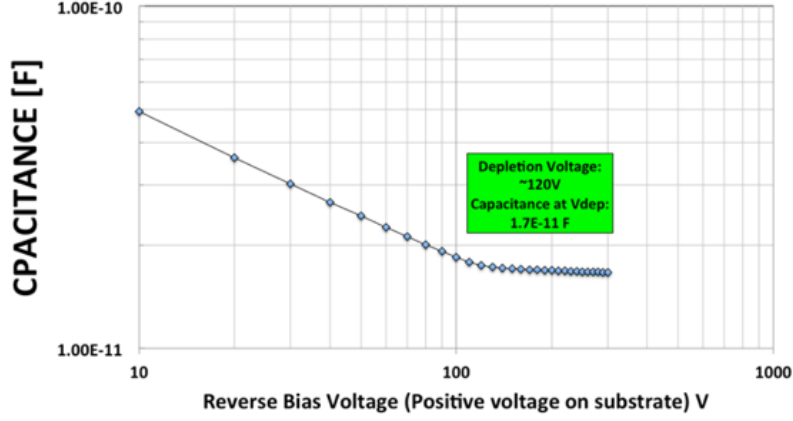


Figure 1: The measured capacitance as a function of the applied bias voltage.

was supplied to the circuitry by a cable with a balun filter, terminated with an SHV connector. The silicon diode output signal is read out through an SMA connector electrically grounded to the box. The dark current was measured at several values of the bias voltage. The maximum value of the dark current was less than 1.0 nA at  $-500$  V, which is the largest bias voltage used in the measurements reported in this paper. The silicon box and bench test setup are presented in Figure 2.

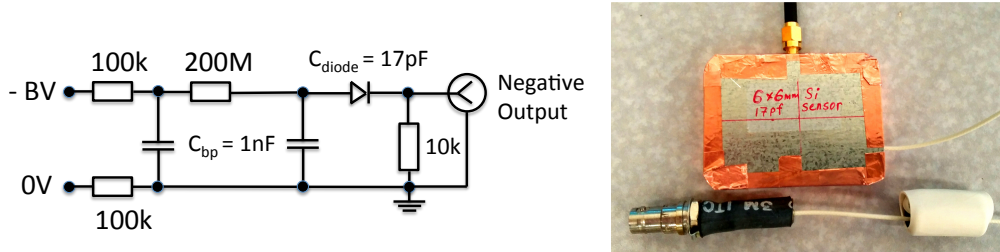


Figure 2: The electric diagram for the silicon diode connections (left). External view of the box with silicon diode, and the bias voltage connection is shown below it (right).

The signals from the silicon sensor were amplified by two fast, high-bandwidth pre-amplifiers connected in series. The first amplifier is an ORTEC VT120C pre-amplifier, and the second amplifier is a Hamamatsu C5594 amplifier. Using a pulse-generator, we measured the combined gain of the two amplifiers in series as a function of the input signal amplitude and found some degree of non-linearity for typical signals produced by the silicon sensor under study, and we corrected for them.

### 3. Test-beam Setup and Experimental Apparatus

We performed the test-beam measurements at the Fermilab Test-beam Facility (FTBF) which provided a proton beam from the Fermilab Main Injector accelerator at 120 GeV,

and secondary beams composed of electrons, pions, and muons of energies ranging from 4 GeV to 32 GeV. A simple schematic diagram of the experimental setup is shown in Figure 3. A small plastic scintillator of transverse dimensions  $1.8 \text{ mm} \times 2 \text{ mm}$  is used as a trigger counter to initiate the read out of the data acquisition (DAQ) system and to select incident beam particles from a small geometric area, allowing us to center the beam particles on the silicon sensor. Next, we place a stack of tungsten absorbers of various thicknesses for measurements of the longitudinal profile of the electromagnetic shower. The silicon pad sensor is located within a metal box covered by copper foil, and is placed immediately downstream of the absorber plates. Finally, a Photek 240 micro-channel plate photomultiplier detector [1–4] is placed furthest downstream, and serves to provide a very precise reference timestamp. Its precision was previously measured to be less than 10 ps [3]. A photograph showing the various detector components is presented in Figure 4. A differential Cherenkov counter is located further upstream of our experimental setup and provides additional particle identification capability. More details of the experimental setup are described in our previous studies using the same experimental facility in references [1–4].

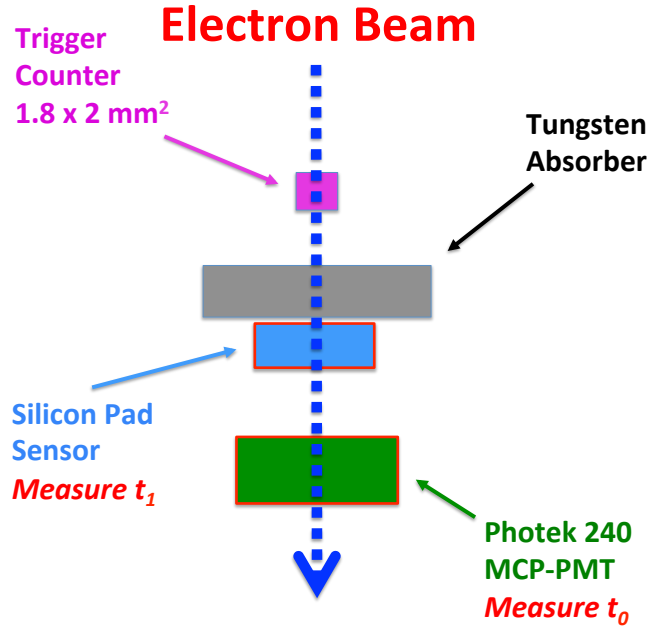


Figure 3: A schematic diagram of the test-beam setup is shown. The  $t_0$  and  $t_1$  are defined in Section 4.

The DAQ system is based on a CAEN V1742 digitizer board [9], which provides digitized waveforms sampled at 5 GS/s. The metal box containing the silicon sensor was located on a motorized X-Y moving stage allowing us to change the location of the sensor in the plane transverse to the beam at an accuracy better than 0.1 mm. A nominal bias voltage of 500 V was applied to deplete the silicon sensor in most of the studies shown below, unless noted otherwise.

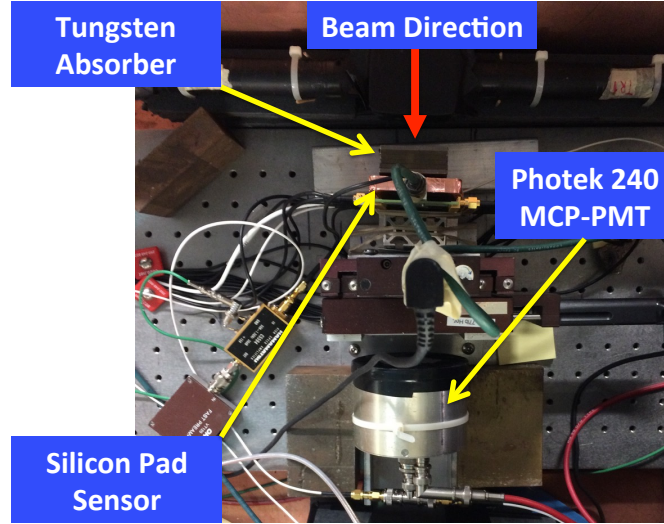


Figure 4: Test beam setup.

#### 4. Test Beam Measurements and Results

Measurements were performed during December 2015, using the primary 120 GeV proton beam, and secondary beams provided for the FTBF. Secondary beams with energies ranging from 4 GeV/c<sup>2</sup> to 32 GeV/c<sup>2</sup> were used. Electron purity for those beams ranges between 70% at the lowest energy to about 10% at the highest energy. Stacks of tungsten plates with varying thicknesses were placed immediately upstream of the silicon device in order to measure the response along the longitudinal direction of the electromagnetic shower. The radiation length of tungsten is 3.5 mm, and the Moliere radius is 9.3 mm. The tungsten plate size is sufficient to fully contain the shower in the transverse dimension. Signals from the silicon sensor and the Photek MCP-PMT are read out and digitized by the CAEN V1742 digitizer, and example signal waveforms are shown in Fig. 5. The signal pulse in the silicon sensor has a rise time of about 1.5 ns, and a full pulse width of around 7 ns. This rise time is consistent with a time constant of a silicon sensor coupled to a 50 Ohm amplifier.

The CAEN digitizer is voltage and time calibrated using the procedure described in Ref. [10]. The total collected charge for each signal pulse is computed by integrating a 10 ns window around the peak of the pulse. The time for the reference Photek MCP-PMT detector is obtained by fitting the peak region of the pulse to a Gaussian function and the mean parameter of the Gaussian is assigned as the timestamp  $t_0$ . The time for signals from the silicon sensor is obtained by performing a linear fit to the rising edge of the pulse and the time at which the pulse reaches 30% of the maximum amplitude is assigned as its timestamp  $t_1$ . We measured the electronic time resolution of the CAEN V1742 digitizer as  $\sim 4$  ps and neglected its impact on the timing measurements described below.

Electrons were identified using a combination of the gas Cherenkov counter provided by the FTBF and the signal amplitude in the Photek detector located further downstream

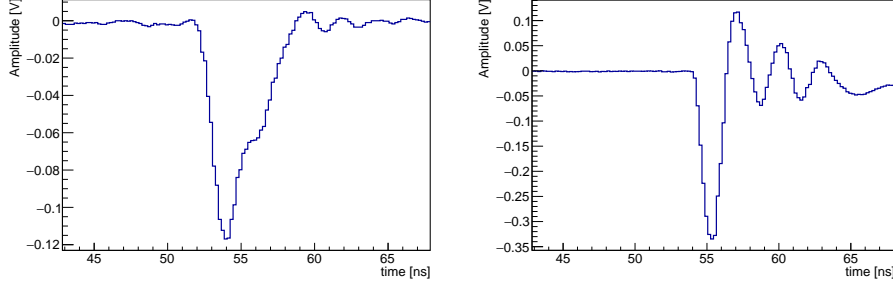


Figure 5: Examples of the signal pulse waveform for the silicon sensor (left) and the Photek MCP-PMT (right) digitized by CAEN V1742 digitizer board. The bias voltage applied to the silicon pad sensor is 500 V.

of the silicon sensor. Electromagnetic showers induced by electrons produce significantly larger signals in the Photek MCP-PMT, while pions produce much smaller signals. After imposing the electron identification requirements the electron purity is between 80% and 90% for all beam conditions.

We begin by establishing the signal characteristics of a minimum-ionizing particle (MIP) using beams of 120 GeV protons and 8 GeV electrons with no absorbers upstream of the silicon pad sensor. To separate MIP signals from noise, we first collect data events with no beam and random trigger. The charge distribution for these noise runs is presented in Fig. 6. As expected, the charge distribution is centered at 0, and the RMS is about 2 fC.

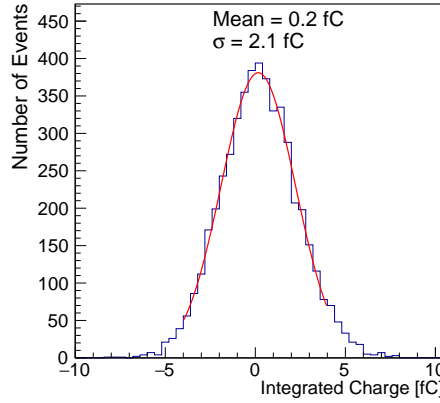


Figure 6: The distribution of charge integrated in the silicon sensor is shown for data events with no beam and random trigger.

In Figure 7, we show silicon sensor response to 120 GeV protons and 8 GeV electrons without any absorber. We observe very similar response for these two cases, and measure peak integrated charge of 4.5 fC and 5.0 fC respectively. The measured signal is corrected for the gain of the amplifiers used, and hence is the output charge of the

152 silicon sensor. We expect peak charge of 28,000 and 31,000 electron-hole pairs in a 325  
 153  $\mu\text{m}$  thick silicon detector for ionizing particles with Lorentz factor  $\gamma = 120$  (protons) and  
 154 16,000 (electrons) [11], which is in a good agreement with the measured values. Having  
 155 established the absolute scale of the response using single particles, in our remaining  
 156 studies we normalize all charge measurements to the 120 GeV proton signal, which we  
 157 refer to in the following as  $Q_{\text{MIP}}$ .

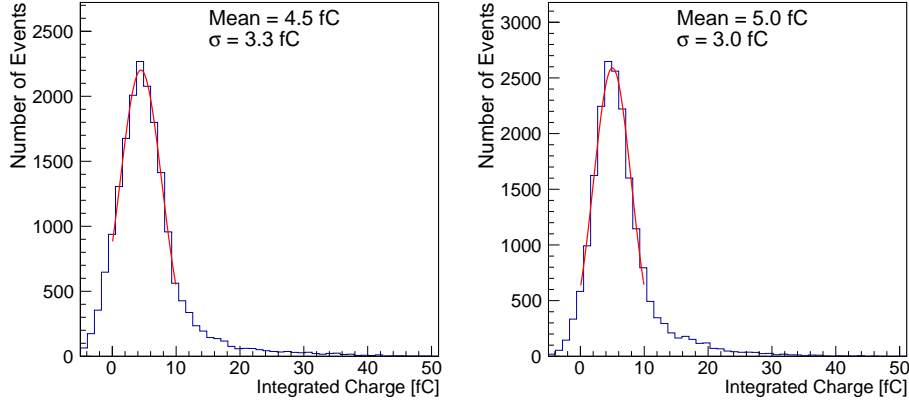


Figure 7: The distribution of charge integrated in the silicon sensor is shown for a beam of 120 GeV protons (left) and 8 GeV electrons (right) without any absorber upstream of the silicon sensor. These conditions mimic the response of the silicon sensor to a minimum-ionizing particle. All triggered events were used in these distributions.

158 We study the response of the silicon sensor to electron beams of various energies  
 159 after 6 radiation lengths ( $X_0$ ) of tungsten absorber. The silicon sensor is expected to  
 160 be sensitive to the number of secondary electrons produced within the electromagnetic  
 161 shower, and therefore its response is expected to scale up with higher incident electron  
 162 energy. In Figure 8, we show an example of the integrated charge distribution measured  
 163 in the silicon sensor after 6 radiation lengths of tungsten, for runs with 32 GeV electrons.  
 164 We show the mean and RMS of these distributions as a function of incident electron beam  
 165 energy in Figure 8. The uncertainties plotted show the RMS of the charge distribution.  
 166 Since the electron beam profile and purity varies at different beam energies, we collected  
 167 between 10 and 50 thousand events for each beam energy, in order to ensure sufficiently  
 168 large data samples. We observe a fairly linear dependence between the measured charge  
 169 and the incident beam energy, for beam energies between 4 GeV and 32 GeV.

170 We also measure the time resolution between the silicon sensor and the Photek MCP-  
 171 PMT, by measuring the standard deviation of the gaussian fit to the distribution of  
 172  $\Delta t = t_0 - t_1$ . We observe a systematic dependence of  $\Delta t$  on the total charge measured  
 173 in the silicon detector, as shown on the left panel in Figure 9. This dependence on the  
 174 integrated charge of the amplified signal was reproduced when we connected the output  
 175 of the pulse generator to the same amplifiers as used in the measurements. We perform  
 176 a correction to  $\Delta t$  for each event using the measured charge in the silicon sensor. This  
 177 procedure is referred to in the following as *time calibration*. The correction is obtained  
 178 from a second degree polynomial fit to the distribution of the  $\Delta t$  versus total charge

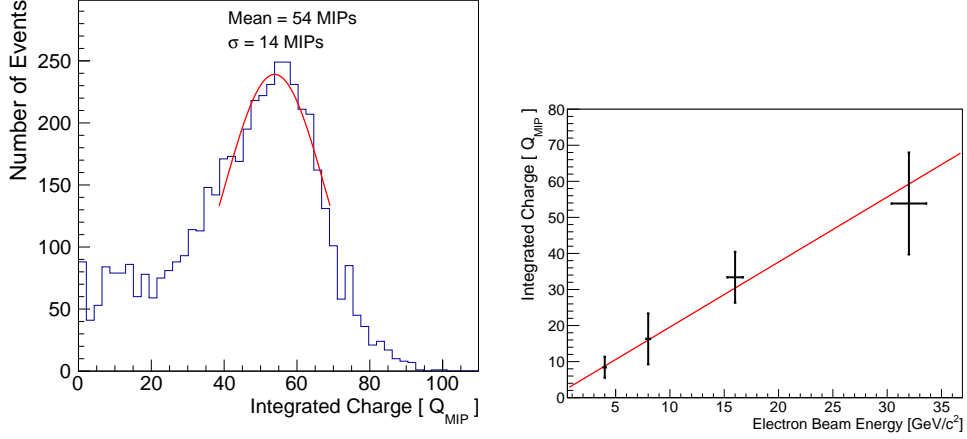


Figure 8: Left: An example of the distribution of integrated charge in the silicon sensor shown in units of charge measured for a MIP. Right: The integrated charge in the silicon sensor expressed in units of the charge measured for a MIP is shown as a function of the electron beam energy. The uncertainty bands show the RMS of the measured charge distribution. The red line is the best fit to a linear function..

collected in the silicon sensor, as shown in Figure 9. We verify that the time calibration flattens the dependence of the time measurement on the integrated charge, as shown on the right panel of Figure 9, and improves the time resolution measurement by 30 – 35%. All time resolution measurements in the rest of this study are performed after time calibration. An example of a corrected  $\Delta t$  distribution for 32 GeV electrons after  $6 X_0$  is shown on the left of Figure 10. Other than the electron identification requirements, no additional selection requirements on the amplitude of the signal in the silicon sensor were made. The dependence of the measured time resolution on the beam energy is shown on the right of Figure 10. We observe an improvement in the time resolution as beam energy increases, and achieve a time resolution of 23 ps for the 32 GeV electron beam.

Furthermore, we study the response and time resolution of the silicon sensor along the longitudinal direction of the shower development. We measure the integrated charge and the time resolution as a function of the absorber thickness and present the results in Figure 11, for electron beam energy of 8 GeV. A typical longitudinal shower profile is observed, consistent with previous studies performed using a secondary emission calorimeter prototype based on MCP's [3], as well as independent studies of silicon-based calorimeter prototypes [12]. The RMS of the integrated charge distribution at each absorber thickness is relatively large, due to the small transverse size of the active element used in the experiment. We also observe that the time resolution improves as the shower develops towards its maximum in the longitudinal direction.

Finally, we studied the dependence of the time resolution as a function of the bias voltage applied to deplete the silicon sensor. The measurements are shown in Figure 12 for 16 GeV electrons after  $6 X_0$  of tungsten absorber. We find that the time resolution improves as the bias voltage is increased, which is expected on the basis of increased velocity of electrons and holes in silicon at larger bias voltage.



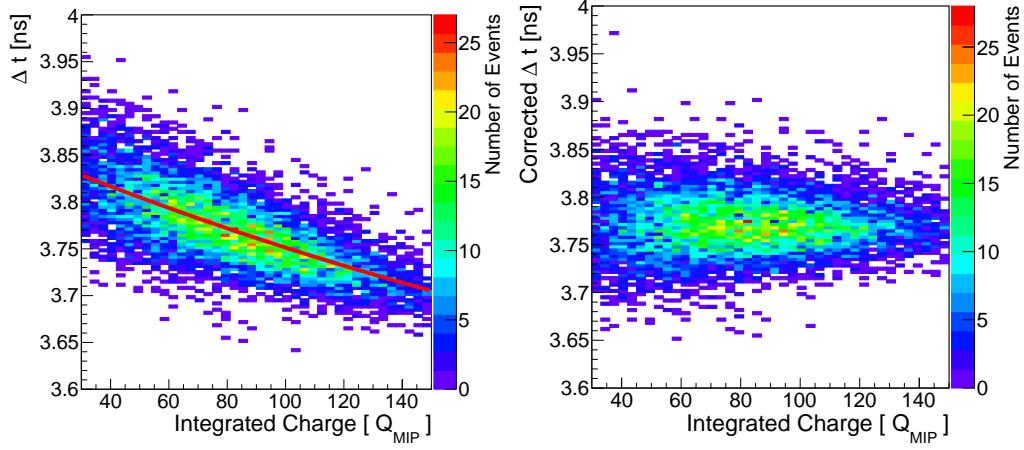


Figure 9: The dependence of  $\Delta t$  on the integrated charge in the silicon sensor is shown on the left. The red curve represents the fit to the profile plot of the two dimensional distribution, and is used to correct  $\Delta t$  for this effect. On the right, we show the corresponding two dimensional distribution after performing the correction. A 16 GeV electron beam is used, and the silicon sensor is placed after  $6 X_0$  of tungsten absorber.

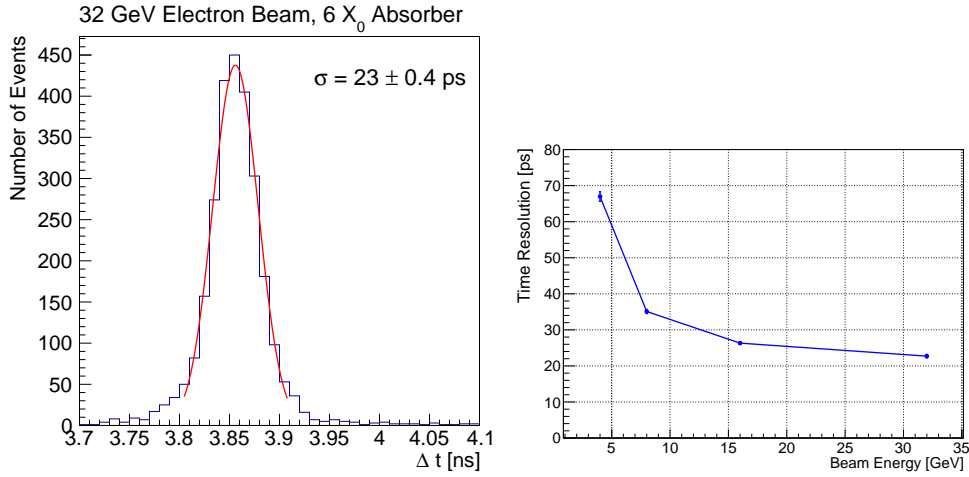


Figure 10: Left: The distribution of  $\Delta t$  between the silicon sensor and the Photek MCP-PMT. A 32 GeV electron beam is used, and the silicon sensor is placed after  $6 X_0$  of tungsten absorber. Right: The measured time resolution between the silicon sensor and the Photek MCP-PMT reference is shown as a function of the electron beam energy. The silicon sensor is placed after  $6 X_0$  of tungsten absorber.

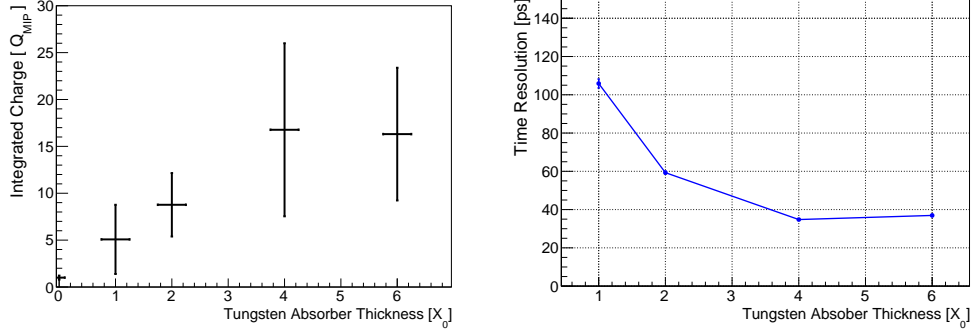


Figure 11: On the left, the integrated charge in the silicon sensor expressed in units of the charge measured for MIPs is shown as a function of the absorber (W) thickness measured in units of radiation lengths ( $X_0$ ). The electron beam energy was 8 GeV. The uncertainty bands show the RMS of the measured charge distribution. On the right, the time resolution between the silicon sensor and the Photek MCP-PMT reference is shown as a function of the absorber thickness.

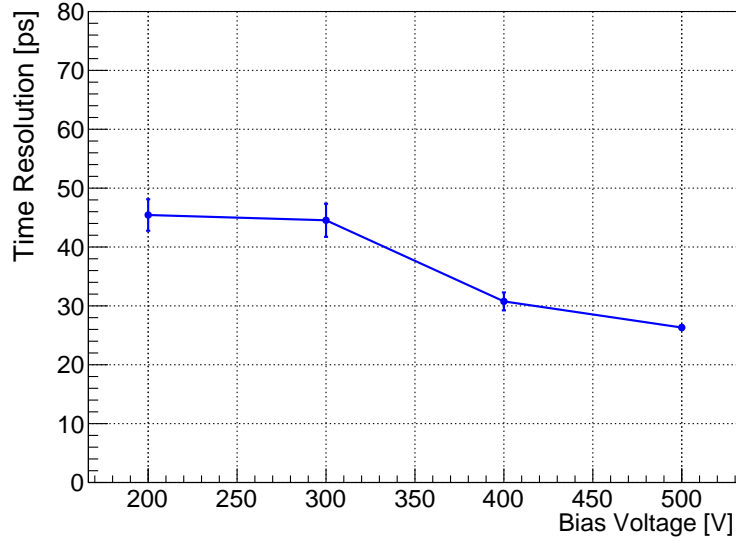


Figure 12: The time resolution between the silicon sensor and the Photek MCP-PMT reference is shown as a function of bias voltage applied on the silicon sensor. The electron beam energy was 16 GeV, and the silicon sensor is placed after 6  $X_0$  of tungsten absorber.

## 5. Discussion

From Figures 6 and 7, we observe that the noise of the prototype system is sufficiently low to extract signals from MIPs. Comparing the RMS of the noise distribution with the mean of the MIP signal, we find a signal-to-noise ratio around 2 to 2.5. A rough estimate from Figure 7 demonstrates that the efficiency to detect 120 GeV protons and 8 GeV electrons with no absorber present is larger than 80%. Based on the measurements for MIPs, we derive signal distributions for electromagnetic showers normalized to MIP response, and observe a relatively linear response to the electron beam energy in the range from 4 GeV to 32 GeV after 6  $X_0$  of tungsten absorber, as shown in Figure 10. We also measure a longitudinal shower profile in Figure 11 that is consistent with similar past measurements.

Our results show that the time stamp associated with electromagnetic showers induced by electrons with energy between 20 GeV and 30 GeV can be measured with a precision better than 25 ps. We find that the time response of the amplifier needs to be well calibrated in order to achieve this result. Subtracting 13 ps for the resolution of the reference Photek MCP-PMT detector measured in showers [3] yields a precision close to 20 ps. Moreover, we observe an improvement of the time resolution with the energy of the electron, and more generally with an increase in the signal amplitude. These measurements demonstrate that a calorimeter based on silicon sensors as the active medium can achieve intrinsic time resolution at the 20 ps level, as long as noise is kept under control. Time jitter arising from intrinsic properties of the silicon sensor is demonstrated to be well below the 20 ps level.

## 6. Conclusion

The best time resolution of 23 ps for a silicon sensor was achieved with a 32 GeV beam and with the silicon sensor placed after 6 radiation lengths of tungsten absorber. Based on our calibration data for the response of the silicon sensor to MIPs, this measurement corresponds roughly to an average of 54 secondary particles registered from the electromagnetic shower. We observe a roughly linearly increasing response as the energy of the electron beam is increased, and we observe a longitudinal shower profile consistent with similar past measurements. This result yields further encouragement to use silicon for active layers in calorimeters, as is planned for example for the CMS Phase 2 upgrade [6], and explicitly demonstrates the opportunity to use silicon for timing measurements in future calorimeters. To continue, we plan to extend our studies to more realistic prototypes covering larger transverse and longitudinal regions of the electromagnetic shower and using multiple channels.

## 7. Acknowledgements

Operated by Fermi Research Alliance, LLC under Contract No. DE-AC02-07CH11359 with the United States Department of Energy. Supported by funding from California Institute of Technology High Energy Physics under Contract DE-SC0011925 with the United States Department of Energy. We thank the FTBF personnel for very good beam conditions during our test beam time. We also appreciate the technical support of the Fermilab SiDet department for the production of high quality silicon samples.

## References

- [1] D. Anderson, A. Apresyan, A. Bornheim, J. Duarte, C. Pena, A. Ronzhin, M. Spiropulu, J. Trevor, and S. Xie, "On Timing Properties of LYSO-Based Calorimeters," *Nucl. Instrum. Meth. A*, vol. 794, pp. 7–14, 2015.
- [2] A. Ronzhin, S. Los, E. Ramberg, M. Spiropulu, A. Apresyan, S. Xie, H. Kim, and A. Zatserklyaniy, "Development of a new fast shower maximum detector based on microchannel plates photomultipliers (MCP-PMT) as an active element," *Nucl. Instrum. Meth. A*, vol. 759, pp. 65 – 73, 2014.
- [3] A. Ronzhin, S. Los, E. Ramberg, A. Apresyan, S. Xie, M. Spiropulu, and H. Kim, "Study of the timing performance of micro-channel plate photomultiplier for use as an active layer in a shower maximum detector," *Nucl. Instrum. Meth. A*, vol. 795, pp. 288 – 292, 2015.
- [4] A. Ronzhin, S. Los, E. Ramberg, A. Apresyan, S. Xie, M. Spiropulu, and H. Kim, "Direct tests of micro channel plates as the active element of a new shower maximum detector," *Nucl. Instrum. Meth. A*, vol. 795, pp. 52 – 57, 2015.
- [5] L. Brianza, F. Cavallari, D. Del Re, S. Gelli, A. Ghezzi, C. Gotti, P. Govoni, C. Jorda Lopez, A. Martelli, B. Marzocchi, P. Meridiani, G. Organtini, R. Paramatti, L. Pernie, S. Pigazzini, S. Rathlou, C. Rovelli, F. Santanastasio, T. Tabarelli de Fatis, N. Trevisani, "Response of microchannel plates to single particles and to electromagnetic showers," *Nucl. Instrum. Meth. A*, vol. 797, pp. 216 – 221, 2015.
- [6] J. Butler, D. Contardo, M. Klute, J. Mans, and L. Silvestris, "Technical Proposal for the Phase-II Upgrade of the CMS Detector," Tech. Rep. CERN-LHCC-2015-010. LHCC-P-008, CERN, Geneva, Jun 2015.
- [7] C. Adloff, J. Blaha, J. J. Blaising, C. Drancourt, A. Espargiliere, R. Galione, N. Geffroy, Y. Karyotakis, J. Prast, and G. Vouters, "Tests of a particle flow algorithm with CALICE test beam data," *JINST*, vol. 6, p. P07005, 2011.
- [8] [https://www.hamamatsu.com/resources/pdf/ssd/e10\\_handbook\\_for\\_high\\_energy.pdf](https://www.hamamatsu.com/resources/pdf/ssd/e10_handbook_for_high_energy.pdf).
- [9] <http://www.caen.it/csite/CaenProd.jsp?parent=11&idmod=661>.
- [10] H. Kim, C.-T. Chen, N. Eclov, A. Ronzhin, P. Murat, E. Ramberg, S. Los, W. Moses, W.-S. Choong, and C.-M. Kao, "A new time calibration method for switched-capacitor-array-based waveform samplers," *Nucl. Instrum. Meth. A*, vol. 767, pp. 67 – 74, 2014.
- [11] K. A. Olive *et al.*, "Review of Particle Physics," *Chin. Phys.*, vol. C38, p. 090001, 2014.
- [12] S. Muhuri, S. Mukhopadhyay, V. B. Chandratre, M. Sukhwani, S. Jena, S. A. Khan, T. K. Nayak, J. Saini, and R. N. Singaraju, "Test and characterization of a prototype silicon-tungsten electromagnetic calorimeter," *Nucl. Instrum. Meth. A*, vol. 764, pp. 24 – 29, 2014.